2017

Electrochemically Inert g-C3N4 Promotes Water Oxidation Catalysis

Yaping Chen
University of Wollongong, yc463@uowmail.edu.au

Qian Zhou
University of Wollongong, qz704@uowmail.edu.au

Guoqiang Zhao
University of Wollongong, gz815@uowmail.edu.au

Zhenwei Yu
University of Wollongong, zy139@uowmail.edu.au

Xiaolin Wang
University of Wollongong, xiaolin@uow.edu.au

See next page for additional authors

Publication Details

Chen, Y., Zhou, Q., Zhao, G., Yu, Z., Wang, X., Dou, S. Xue. & Sun, W. (2017). Electrochemically Inert g-C3N4 Promotes Water Oxidation Catalysis. Advanced Functional Materials, 28 (5), 1705583-1-1705583-7.

Electrochemically Inert g-C3N4 Promotes Water Oxidation Catalysis

Abstract

Electrode surface wettability is critically important for heterogeneous electrochemical reactions taking place in aqueous and nonaqueous media. Herein, electrochemically inert g-C 3 N 4 (GCN) is successfully demonstrated to significantly enhance water oxidation by constructing a superhydrophilic catalyst surface and promoting substantial exposure of active sites. As a proof-of-concept application, superhydrophilic GCN/Ni(OH) 2 (GCNN) hybrids with monodispersed Ni(OH) 2 nanoplates strongly anchored on GCN are synthesized for enhanced water oxidation catalysis. Owing to the superhydrophilicity of functionalized GCN, the surface wettability of GCNN (contact angle 0°) is substantially improved as compared with bare Ni(OH) 2 (contact angle 21°). Besides, GCN nanosheets can effectively suppress Ni(OH) 2 aggregation to help expose more active sites. Benefiting from the well-defined catalyst surface, the optimal GCNN hybrid shows significantly enhanced electrochemical performance over bare Ni(OH) 2 nanosheets, although GCN is electrochemically inert. In addition, similar catalytic performance promotion resulting from wettability improvement induced by incorporation of hydrophilic GCN is also successfully demonstrated on Co(OH) 2 . The present results demonstrate that, in addition to developing new catalysts, building efficient surface chemistry is also vital to achieve extraordinary water oxidation performance.

Disciplines

Engineering | Physical Sciences and Mathematics

Publication Details

Chen, Y., Zhou, Q., Zhao, G., Yu, Z., Wang, X., Dou, S. Xue. & Sun, W. (2017). Electrochemically Inert g-C3N4 Promotes Water Oxidation Catalysis. Advanced Functional Materials, 28 (5), 1705583-1-1705583-7.

Authors

Yaping Chen, Qian Zhou, Guoqiang Zhao, Zhenwei Yu, Xiaolin Wang, Shi Xue Dou, and Wenping Sun

DOI: 10.1002/((please add manuscript number))

Article type: Full Paper

Electrochemically Inert g-C_3N_4 Promotes Water Oxidation Catalysis

*Yaping Chen, Qian Zhou, Guoqiang Zhao, Zhenwei Yu, Xiaolin Wang, Shi Xue Dou, Wenping Sun**

Y.P. Chen, Q. Zhou, G.Q. Zhao, Z.W. Yu, Prof. X.L. Wang, Prof. S. X. Dou, Dr. W.P. Sun
Institute for Superconducting and Electronic Materials, Australian Institute of Innovative Materials, University of Wollongong, Wollongong, NSW 2522, Australia
E-mail: wenping@uow.edu.au

Abstract: Electrode surface wettability is critically important for heterogeneous electrochemical reactions taking place in aqueous and non-aqueous medium. Herein, electrochemically inert g-C_3N_4 (GCN) was successfully demonstrated to significantly enhance water oxidation by constructing a superhydrophilic catalyst surface and promoting substantial exposure of active sites. As a proof-of-concept application, superhydrophilic GCN/$Ni(OH)_2$ (GCNN) hybrids with monodispersed $Ni(OH)_2$ nanoplates strongly anchored on GCN were synthesized for enhanced water oxidation catalysis. Owing to the superhydrophilicity of functionalized GCN, the surface wettability of GCNN (contact angle 0°) was substantially improved as compared with bare $Ni(OH)_2$ (contact angle 21°). Besides, GCN nanosheets can effectively suppress $Ni(OH)_2$ aggregation to help expose more active sites. Benefiting from the well-defined catalyst surface, the optimal GCNN hybrid showed significantly enhanced electrochemical performance over bare $Ni(OH)_2$ nanosheets, although GCN is electrochemically inert. In addition, similar catalytic performance promotion resulting from wettability improvement induced by incorporation of hydrophilic GCN was also successfully demonstrated on $Co(OH)_2$. The present results demonstrate that, in addition to developing new catalysts, building efficient surface chemistry is also vital to achieve extraordinary water oxidation performance.

Keywords: Graphitic carbon nitride; Wettability; Nickel hydroxide; Oxygen evolution reaction

1. Introduction

Recently, ever-increasing research interest has been focused on developing alternative strategies to efficiently utilize sustainable renewable energy worldwide. In addition to grid-scale energy storage, energy conversion, which means converting renewable energy into various chemical energies, is another important avenue. Water electrolysis (electrochemical water splitting) is one typical chemical process that converts electricity derived from renewable energy into hydrogen, and also presents a clean and potentially cost-effective pathway to achieve renewable energy conversion.[1] Compared with hydrogen evolution reaction (HER), oxygen evolution reaction (OER) is much more sluggish because four electrons need to be removed to form oxygen, and hence water electrolysis efficiency is greatly hindered by kinetically sluggish OER. On the other hand, OER is also an important half reaction involved in rechargeable metal–air batteries, and the corresponding OER reaction kinetics determines the battery performance as well.[2] Therefore, developing highly-efficient catalysts for OER are extremely urgent to address the challenges in artificial water-splitting systems and metal-air batteries.[3] Some noble-metal catalysts such as Ru- and Ir-based materials are state-of-the-art OER electrocatalysts; however, the considerable scarcity and high cost seriously limit their practical applications.[4] It is thus critical to explore low-cost and stable alternatives with promising catalytic performance towards water oxidation. To date, numerous efforts have been undertaken to design non-precious OER catalysts,[5] and non-precious metal-based oxides,[6] hydroxides,[7] and carbonaceous materials[8] have drawn much reacearch attention. In particular, Ni-based hydroxides and oxides demonstrated outstanding OER catalytic activities with a low overpotential and high electrolysis current in alkaline electrolytes.[5a, 7a]

In order to further enhance the electrocatalytic activity of the aforementioned Ni-based catalysts, current strategies mainly focuse on heteroatom doping, designing and synthesizing highly efficient nanostructures/nanocomposites.[7b, 7c, 9] It should be mentioned that most

approaches aim to improve the intrinsic activity, expose more active sites, and/or enhance charge transfer ability of the catalysis. As is already known, in addition to exposed active sites and charge transfer ability, the electrocatalytic performance of the heterogeneous catalysis has close correlation with the adsorption and desorption properties of the electrode surface, which determine the mass-diffusion kinetics of both the reactants and products. The adsorption of reactants/intermediate and desorption of products on the catalyst surface is forcefully affected by the catalyst wettability.[10] Bhaumik et al. displayed the hydroxylation of benzene to increase the hydrophobicity, which more profitably adsorbs and transfers the hydrophobic benzene reactant in the triphasic system.[10a] Li et al. successfully achieved enhanced water oxidation catalysis on phosphorylated NiFe hydroxide by tuning catalyst wettability.[10d] In this regard, engineering electrode materials with superwettability has a prominent aspect on promoting electrolyte penetration, mass diffusion and charge transfer as well, thereby achieving enhanced electrocatalytic activity.

Recently, 2D graphitic carbon nitride g-C_3N_4 (GCN) has been widely implemented in the photocatalysis field due to its unique electronic band structure and high physicochemical stability.[11] Some effort has already been made to study GCN-based composites as electrocatalysts for water splitting.[12] It was found that bare GCN is nearly inert for OER and hydrogen evolution reaction (HER), and the delivered catalytic performance is mainly ascribed to the synergistic effect of GCN and the conductive carbonaceous materials (e.g., CNT and graphene). Nevertheless, some unique physicochemical properties of GCN make it an attractive component for constructing high-performance electrocatalysis occurred in aqueous environment. It is worth noting that proton-functionalized GCN nanosheets show excellent water dispersion stability, and this would substantially improve the wettability of the composites containing such GCN nanosheets.[13] Besides, the GCN nanosheets can help achieve good dispersion and hinder agglomeration of active materials, ensuring substantial exposure of the active sites. Moreover, the excellent chemical stability enables GCN to

function as a robust substrate for active materials towards durable performance.[14] Based on the aforementioned statement, we speculate that the catalyst hydrophicility would be greatly improved over bare $Ni(OH)_2$ by constructing GCN/$Ni(OH)_2$ (GCNN) hybrid. Besides, the introduction of GCN would efficiently realize good dispersion and hinder aggregation of $Ni(OH)_2$. These two unique properties together with the excellent stability of GCN would help the GCNN hybrid to achieve highly efficient and durable water oxidation catalysis. Herein, 2D GCNN hybrid with monodispersed $Ni(OH)_2$ nanoplates strongly coupled with GCN nanosheets were prepared by a facile one-pot hydrothermal process. As expected, the $Ni(OH)_2$ nanoplates are uniformly dispersed on GCN nanosheets, and the GCNN hybrid shows superhydrophilicity. Although the intrinsic electrocatalytic ability of GCN is negligible and less catalytic active material $Ni(OH)_2$ is present, the GCNN hybrid delivers significantly enhanced electrocatalytic ability for OER as compared with bare ultrathin $Ni(OH)_2$ nanosheets. The excellent electrochemical performance suggests that, in addition to improve intrinsic catalytic ability and expose more active sites, engineering an efficient catalyst surface is also vital to gain accelerated catalytic reaction kinetics.

2. Results and discussion

The schematic illustration of the synthetic route toward 2D GCNN hybrids is displayed in **Figure S1** (Supporting Information). Firstly, Ni^{2+} ions are intercalated into the interlamination via ultrasonication treatment and this could effectively promote the exfoliation of functionalized GCN with lots of protons and aminos.[15] During the hydrothermal process, the adsorbed Ni^{2+} cations participate into the homogeneous precipitation reaction and form $Ni(OH)_2$ nanoplates on GCN nanosheets. It should be noted that the hydrothermal process also facilitates the exfoliation of GCN.

Figure 1a shows the X-ray diffraction (XRD) pattern of the as-prepared GCNN:65 (65 wt% $Ni(OH)_2$) nanocomposite. It can be seen that the XRD pattern contains typical diffraction peaks of hexagonal phase α-$Ni(OH)_2$ and GCN, reflecting that the formation of GCNN.[16]

Notably, the intensity of the GCN (002) peak at 27.4°, corresponding to the characteristic interlayer stacking structure, is evidently reduced compared to bulk GCN (**Figure S2**, Supporting Information), indicating the formation of few-layered nanosheets.[13] Besides, all the other GCNN samples possess similar crystal structures (**Figure S2**, Supporting Information). Fourier-transform infrared spectroscopy (FTIR) (**Figure S3**, Supporting Information) further confirms the formation of GCNN:65. The broad band locating from 3200 cm^{-1} to 3600 cm^{-1} corresponds to the O-H vibration of hydrogen-bonded hydroxyl groups of $Ni(OH)_2$.[17] The absorption band located at 2202 cm^{-1} can be assigned to the typical vibration of C≡N bonds in the OCN^- anions produced during the urea hydrolysis.[18] The distinctive stretch mode of aromatic CN heterocycles from 1100 to 1600 cm^{-1} coupled with the breathing mode of the triazine units at 810 cm^{-1} evidence the presence of GCN.[19] Scanning electron microscopy (SEM) and transmission electron microscopy (TEM) characterizations were conducted to investigate the sample morphology. The SEM (**Figure S4**a, Supporting Information) result suggests that GCNN:65 have flexible nanosheets morphology. As shown in Figure 1b, $Ni(OH)_2$ nanoplates (around 10-30 nm in lateral size) are strongly coupled with GCN nanosheets. As a functional substrate similar to graphene-like structures, the GCN nanosheets could effectively prevent $Ni(OH)_2$ nanoplates from agglomeration, ensuring the maximum exposure of active sites. GCNN:44, GCNN:60 and GCNN:77 possess similar nanosheet morphology with $Ni(OH)_2$ nanoplates anchored on GCN nanosheets (**Figure S5**, Supporting Information). The $Ni(OH)_2$ nanoplates tend to aggregate together with decreasing the content of GCN, which would definitely decrease the density of active sites. In contrast, bare $Ni(OH)_2$ nanosheets synthesized via similar process show flexible nanosheets morphology, which is several micro in lateral size (**Figure S4b**, Supporting Information). The selected area electron diffraction (SAED) pattern can be fully indexed to the hexagonal α-$Ni(OH)_2$ phase (**Figure 1c**). A lattice spacing of 0.236 nm determined from the HRTEM image (**Figure 1d**) can be assigned to the (101) plane of $Ni(OH)_2$. Furthermore, the scanning

transmission electron microscopy (STEM) elemental mappings (**Figure 1e**) show the uniform distribution of C, N, O and Ni across the GCNN:65 composite nanosheet, indicating the uniform hybridization of $Ni(OH)_2$ nanoplates and GCN nanosheets. The elemental composition and chemical states of GCNN:65 nanocomposite was also investigated by X-ray photoelectron spectra (XPS) analysis. The survey spectrum (**Figure 2**a) reveals the co-occurrence of C, N, O and Ni elements.[20] C 1s spectra of GCN and GCNN:65, as shown in **Figure 2b**, show totally distinct profiles. The peaks of C 1s at 284.7 eV and 288.3 eV can be assigned to the typical graphitic sp^2 C–C and C–N=C bonds for GCN, respectively.[21] Two oxygenic groups (C-O at 286.2 eV and C=O at 288.7 eV) appear in GCNN:65, which can be attributed to the formation of oxygen functional bridges between $Ni(OH)_2$ nanoplates and GCN. Notably, C–O–Ni band rather than C–Ni–O is formed since the C–Ni bonds at 283.5 eV is absented in the C 1s spectrum.[22] The O 1s peak at 531.7 eV as shown in **Figure S6** (Supporting Information) confirms the presence of the O–Ni bond.[22-23] The present results suggest the existence of chemical bonding between GCN and $Ni(OH)_2$. The N 1 s spectrum (**Figure 2c**) shows three peaks at binding energies of 398.5, 399.6 and 400.9 eV, which is corresponding to the graphitic N, pyrrolic N and pyridinic N in GCN, respectively.[12b] In **Figure 2d**, besides two satellite peaks, two peaks with binding energies of 855.7 and 873.3 eV can be assigned to Ni $2p_{3/2}$ and Ni $2p_{1/2}$, respectively, and the spin-energy separation of 17.6 eV is the characteristic of Ni^{2+} in $Ni(OH)_2$.[24]

The electrocatalytic performances of 2D GCNN hybrids together with bare $Ni(OH)_2$ and GCN for OER were investigated under alkaline conditions using a typical three-electrode system. **Figure 3**a shows the iR-corrected linear sweep voltammetry (LSV) curves conducted in 1 M KOH aqueous solution at a scan rate of 5 mV s^{-1}. In the polarization curves, the peak located at around 1.43 V versus RHE can be ascribed to the redox reaction of Ni^{2+}/Ni^{3+} in $Ni(OH)_2$.[9] Clearly, GCN is inert to the water oxidation reaction, but the catalytic activity of the $Ni(OH)_2$ is dramatically enhanced by incorporating moderate GCN nanosheets. The

catalytic activity of the GCNN composites varies significantly with altering the content of GCN, and GCNN:65 containing around 35 wt.% GCN delivers the best performance. The GCNN:65 requires the lowest overpotential of 290 mV to achieve a current density of 10 mA cm^{-2}, which is significantly decreased as compared with $Ni(OH)_2$ (350 mV). In order to further evaluate the OER kinetics of the catalysts, Tafel plots are obtained from the polarization curves, as presented in Figure 3b. The Tafel slope initially decreases with increasing GCN content and reaches the smallest value for GCNN:65, and then increases accordingly. The Tafel slope of GCNN:65 is determined to be 77 mV dec^{-1}, and is much smaller than that of $Ni(OH)_2$ (103 mV dec^{-1}), confirming superior OER kinetics of GCNN:65. In addition, at a potential of 1.8 V (vs. RHE), GCNN:77, GCNN:65, GCNN:60, GCNN:44 and bare $Ni(OH)_2$ delivers 73, 152, 92, 29 and 55 mA cm^{-2}, respectively (Figure 3d). The performance of GCNN:65 is nearly triple that of $Ni(OH)_2$. In order to clearly distinguish the promotion effect of GCN on the electrocatalytic ability of $Ni(OH)_2$, the LSV curves presenting the mass activity (based on active $Ni(OH)_2$ mass) are plotted, as shown in Figure 3c. Much more significant performance enhancement can be observed when the performance is compared based on active $Ni(OH)_2$ mass. At the same potential of 1.8 V (vs. RHE), the current density is calculated to be 773, 1900, 1249, 540 and 440 mA mg^{-1} for GCNN:77, GCNN:65, GCNN:60, GCNN:44 and bare $Ni(OH)_2$, respectively (Figure 3d). Impressively, the electrochemical performance of active $Ni(OH)_2$ is increased more than three times after incorporating 35 wt% functionalized GCN. Even for the simply mixed GCN-$Ni(OH)_2$:65 sample (35 wt% GCN), it also exhibits improved catalytic performance over $Ni(OH)_2$, and the current density reaches 65 mA cm^{-2} and 823 mA mg^{-1} at 1.8 V (**Figure S7**, Supporting Information). The long-term stability of a catalyst is another crucial factor to consider for commercial applications. Continuous chronoamperometry (CA) at a constant potential of 0.55 V (vs. Ag/AgCl) was carried out in 1 M KOH to evaluate the cycling stability of GCNN:65. As shown in Figure 3e, the current density steadily increases over time and retains 102% of

the initial current (96% of the peak current density) after 10-h operation. In contrast, the current density of $Ni(OH)_2$ at the same potential decays quickly after 1-h operation and eventually only 65% current density is retained. The CV profiles conducted at 10 mv s^{-1} nearly overlap each other over 500 cycles (**Figure S8**, Supporting Information), further revealing the good cycle stability of GCNN:65.

Generally, OER in alkaline solution involves migration of hydroxyl groups, oxidation of hydroxyl groups, and oxygen release. Migration and oxidation of hydroxyl groups takes place at solid-liquid (electrode-electrolyte) interface, and oxygen release occurs at solid-gas (electrode-oxygen) interface. Therefore, developing efficient electrode surface chemistry is of great importance towards enhanced catalytic performances. Basically, the oxidation kinetics of hydroxyl is determined by the intrinsic catalytic activity of the catalyst and the density of the active sites. The efficiency of migration of hydroxyl groups and oxygen release are closely associated with the catalyst wettability. Apparently, for a specific OER catalyst, creating more active sites and engineering superhydrophilic surface are vital to improve the overall electrochemical reaction kinetics. In this work, the GCNN:65 nanocomposite simultaneously has these two key characteristics, and hence delivers substantially improved catalytic performance as compared with bare $Ni(OH)_2$.

Firstly, the incorporation of functionalized GCN effectively prevents $Ni(OH)_2$ from agglomeration, and monodispersed $Ni(OH)_2$ nanoplates are strongly coupled with the ultrathin GCN nanosheets, ensuring the maximum exposure of active sites and high electrochemical active surface areas (ECSA). The ECSA of the catalysts are estimated by determining the double-layer capacitance (C_{DL}) based on CVs measured in a non-Faradaic region (**Figure S9**, Supporting Information). As shown in Figure S8d (Supporting Information), the GCNN:65 hybrid catalyst shows much higher current than that of bare $Ni(OH)_2$ and GCN. The ECSA of GCNN:65, bare $Ni(OH)_2$ and GCN is calculated to be 6.83, 1.25 and 4.85 cm^2, respectively, based on the C_{DL} values of the catalysts, as present in **Figure 4**a. The results suggest that the

ECSA of $Ni(OH)_2$ in GCNN:65 nearly doubles that of bare $Ni(OH)_2$ nanoplates, revealing that more accessible active sites are created after introducing GCN, thereby resulting in greatly enhanced catalytic performance.

Secondly, the surface wettability of GCNN:65 is greatly improved after combining $Ni(OH)_2$ with GCN, resulting in fast diffusion of hydroxyl ions and desorption of oxygen gas. The static contact angle measurements were performed to investigate the surface wettability of the catalysts. $Ni(OH)_2$ is hydrophilic with a contact angle of 21° (Figure 4c). As shown in Figure 4d, the contact angle of GCNN:65 nanocomposite is dramatically decreased to 0° after incorporating functionalized GCN (Figure 4e), suggesting the formation of a superhydrophilic catalyst surface. The simply mixed GCN-$Ni(OH)_2$:65 sample (35 wt% GCN) also has a superhydrophilic surface (**Figure S10**, Supporting Information). Considering that $Ni(OH)_2$ in GCN-$Ni(OH)_2$:65 sample shows nearly identical physicochemical properties, in particular the density of active sites, with bare $Ni(OH)_2$, it can be concluded that the enhanced catalytic performance of GCN-$Ni(OH)_2$:65 (Figure S6, Supporting Information) is induced by the substantially improved wettability. The superhydrophilic surface would ensure fast electrolyte penetration to the catalyst surface and accelerated diffusion of hydroxyl-based reactants.[10d] In addition, the superhydophilic surface is very beneficial to rapid removal of gas bubbles and to maintain sufficient electrode working area.[10b] All the unique functionalities are of great significance to deliver enhanced electrocatalytic performance. Furthermore, as can be seen from the electrochemical impedance spectra (Figure 4b), the charge transfer (R_{ct}) resistance of GCNN:65 is around 5.3 Ω, and it is much smaller than that of $Ni(OH)_2$ (17.6 Ω) and GCN (up to 143.2 Ω) (**Figure S11**, Supporting Information), revealing accelerated charge transfer and surface reaction kinetics at the GCNN:65 electrode/electrolyte interface. The enhanced reaction kinetics of GCNN:65 can be attributed to the synergistic effect of the significantly improved wettability and monodispersed $Ni(OH)_2$ nanoplates with substantial exposure of active sites.

Similar performance promotion resulting from the wettability improvement induced by the incorporation of hydrophilic functionalized GCN is also successfully demonstrated on $Co(OH)_2$. Pure $Co(OH)_2$ nanosheets (**Figure S12**, Supporting Information) and simply mixed GCN-$Co(OH)_2$:65 sample (35 wt% GCN) were prepared and the corresponding OER performances were evaluated in 1 M KOH. As shown in **Figure S13**a and b (Supporting Information), the GCN-$Co(OH)_2$:65 sample exhibits lower overpotential and Tafel slope (332 mV at 10 mA cm^{-2}, 62 mV dec^{-1}) than that of bare $Co(OH)_2$ (388 mV at 10 mA cm^{-2}, 65 mV dec^{-1}), clearly demonstrating improved catalytic performance after incorporating GCN. Obviously, although GCN-$Co(OH)_2$:65 contains less active material, it shows higher current density than bare $Co(OH)_2$ under same operating potentials. Notably, the GCN/$Co(OH)_2$ hybrid will no doubt deliver more exceptional performance if similar well-defined structure like GCNN:65 is prepared. As compared with bare $Co(OH)_2$ (contact angle 22°), the contact angle of GCN-$Co(OH)_2$:65 is 0°, revealing a superhydrophilic surface (Figure S12c and d, Supporting Information). Therefore, it can be concluded that introducing hydrophilic functionalized GCN can significantly promote water oxidation catalysis by delivering a superhydrophilic catalyst surface.

3. Conclusion

In summary, we reported that electrochemically inert functionalized GCN can substantially promote water oxidation catalysis by improving the wettability and active site exposure of the catalysts. As a proof-of-concept demonstration, superhydrophilic GCNN hybrid nanosheets were synthesized towards efficient water oxidation catalysis. In addition to the superhydrophilic catalyst surface, plenty of monodispersed $Ni(OH)_2$ nanoplates were strongly coupled with GCN, ensuring the maximum exposure of active sites. Consequently, the GCNN hybrid with moderate GCN content exhibited significantly enhanced electrocatalytic performance as compared with bare $Ni(OH)_2$ nanosheets. Similar performance enhancement was also successfully demonstrated on $Co(OH)_2$ after integrating with superhydrophilic GCN.

This work opens a new avenue for the development of highly efficient catalysts for electrochemical reactions taking place in aqueous and non-aqueous medium.

4. Experimental

All the chemicals were purchased from Sigma-Aldrich (A.R) and were used as received without further purification.

Preparation of functionalized GCN: Bulk GCN powders were prepared by calcining melamine as precursor in air at 550 °C for 2 h with a heating rate of 2.3 °C min^{-1}. For the functionalization of GCN, bulk GCN powders were dispersed in 6 M HCl with ultrasonication for 1 h, and then stirred for 4 h at room temperature.[13] The functionalized GCN was centrifuged and washed with deionized water for several times.

Preparation of GCNN nanocomposites: The as-prepared samples are named as GCNN:x, where "x" means the mass percentage content of $Ni(OH)_2$ in the hybrid, which is calculated based on the TGA results (**Figure S14**, Supporting Information). Take the synthesis of GCNN:65 for an example, 20 mg functionalized GCN and 250 mg $Ni(NO_3)_2{\cdot}6H_2O$ were dispersed in 15 ml ethylene glycol followed by adding 20 ml deionized water with unltrasonication for 4 h. Then 103.2 mg urea was added into the above mixture under magnetic stirring to become homogeneous suspension. Next, the above reaction mixture was transferred to a Teflon stainless-steel autoclave with a capacity of 50 mL. The autoclave was sealed and heated at 120 °C for 10 h in an electric oven. The resulting products were collected by centrifugation and washed with ethanol and deionized water for three times respectively, and were eventually dried at 60 °C in oven overnight. Similarly, GCNN:x (x=44, 60, 77) was synthesized following the same procedure by adding different quantities of precursors (50, 30, 10 mg GCN, 156.2, 187.5, 281.7 mg $Ni(OH)_2$ and 64.5, 77.4, 116.3 mg urea for GCNN:44, GCNN:60, GCNN:77, respectively).

Preparation of $Ni(OH)_2$ and $Co(OH)_2$: Pure $Ni(OH)_2$ and $Co(OH)_2$ nanosheets were synthesized via a similar hydrothermal process. For $Ni(OH)_2$, 250 mg $Ni(NO_3)_2{\cdot}6H_2O$ and

103.2 mg urea were dissolved in mixed solvent containing15 ml ethylene glycol and 20 ml deionized water under magnetic stirring. For $Co(OH)_2$, 261.9 mg $Co(NO_3)_2 \cdot 6H_2O$ and 252.3 mg hexamethylenetetramine (HMT) worked as precursors instead. Then, the solution was transferred to a Teflon stainless-steel autoclave with a capacity of 50 mL. The autoclave was sealed and heated at 120 °C for 10 h in an electric oven. The resulting products were collected by centrifugation and washed with ethanol and deionized water for three times respectively, and were eventually dried at 60 °C in oven overnight.

Materials Characterization: X-ray diffraction (XRD) was carried out using GBC MMA X-ray diffractometer (λ = 1.5406 Å, 25mA, 40 Kv, step size of 0.02 ° s^{-1}). Fourier transform infrared (FTIR) spectra of the samples employed KBr as the background were determined by a Shimadzu FTIR Prestige-21 spectrometer in the frequency range of 4000–650 cm^{-1} with a resolution of 4 cm^{-1}. The morphology and microstructures of the samples were characterized by the field emission scanning electron microscope (FESEM, JEOL JSM-7500FA) equipped with energy-dispersive X-ray spectroscopy (EDS) and resolution transmission electron microscopy (HRTEM, JEM-2010, working voltage 200 kV) and selected area electron diffraction (SAED). X-ray photoelectron spectroscopy (XPS) measurements were carried out on a Thermo ESCALAB 250Xi instrument, using monochrome Al Ka (*hv* =1486.6 eV) as the X-ray excitation source. Contact angles were measured by Dataphysics OCA15 with 2 μL 1 M KOH solution for each testing. Three different spots per substrate on three different areas were measured. Thermogravimetric analysis (TGA): TGA (Mettler Toledo TGA/DSC 1) were performed from 30 to 780 °C at a heating/cooling rate of 10 °C min^{-1} in air to characterize the thermophysical properties.

Electrochemical measurement: Rotating disk electrode and WaveDriver 20 bipotentiostat/galvanostat system (Pine Instruments) were used for electrochemical measurement. All electrocatalytic measurements were conducted in 1 M KOH aqueous solution employing Ag/AgCl (saturated KCl solution) as the reference electrode, a platinum

wire as the counter electrode, and the glassy carbon electrode (0.196 cm^{-2} of effective working area) coated with different catalysts as the working electrodes. For the preparation of working electrodes, 2 mg catalysts were dispersed in a mixed solution containing 16 µL Nafion solution (Aldrich Co., 5 wt%), 384 µL deionized water and 100 µL isopropanol via sonicating for 30 min to obtain a homogeneous ink. Then 10 µL of the catalyst ink (containing 40 µg of catalyst) was cast onto the polished glassy carbon electrode, and subsequently the electrode was dried in ambient air. During the measurements, the working electrode was constantly rotated at 1600 rpm to remove generated O_2. LSV polarization curves were performed at 5 mV s^{-1} to demonstrate the OER activity. All LSV curves were corrected with 95% iR compensation. Cyclic voltammetry (CV) was first conducted from 1.02 V to 1.62 V vs RHE at a scan rate of 10 mV s^{-1} to activate the catalysts before LSV test. Chronoamperometry measurement was conducted under the same potential of 0.6 V (vs. Ag/AgCl) to study the durability. Electrochemical impedance spectra (EIS) were measured at 0.6 V (vs. Ag/AgCl) in the frequency range of 0.1−100 kHz. The electrochemically active surface area (ECSA) is estimated based on the measured double-layer capacitance (C_{DL}) of the synthesized electrodes in 1 M KOH according to the reported method.[4c] The ECSA values were calculated according to the following equations:

$$i_c = vC_{DL}$$

Where the charging current i_c, is equal to the product of the electrochemical double layer capacitance C_{DL} and the scan rate v.

$$ECSA = \frac{C_{DL}}{C_S}$$

Here we can calculate the ECSA with C_{DL} and a general C_s = 0.04 mF cm^{-2} in 1 M KOH based on a typical reported value.

Acknowledgements

This work was financially supported by the Australian Research Council (ARC) DECRA Grant (DE160100596) and an AIIM FOR GOLD Grant (2017). The authors are deeply thankful to Mr. Borui Liu, for his drawing schematic illustrations and kind help.

Received: ((will be filled in by the editorial staff))

Revised: ((will be filled in by the editorial staff))

Published online: ((will be filled in by the editorial staff))

References

[1] G. Wu, K. L. More, C. M. Johnston, P. Zelenay, *Science* **2011**, 332, 443.

[2] a) M. Zhou, H. L. Wang, S. Guo, *Chem Soc Rev* **2016**, 45, 1273; b) J. Fu, F. M. Hassan, C. Zhong, J. Lu, H. Liu, A. Yu, Z. Chen, *Adv. Mater.* **2017**, 29, 1702526.

[3] Q. Kang, L. Vernisse, R. C. Remsing, A. C. Thenuwara, S. L. Shumlas, I. G. McKendry, M. L. Klein, E. Borguet, M. J. Zdilla, D. R. Strongin, *J. Am. Chem. Soc.* **2017**, DOI: 10.1021/jacs.6b09184.

[4] a) M. E. G. Lyons, L. D. Burke, *J. Chem. Soc., Faraday Trans. 1* **1987**, 83, 299; b) S. Ardizzone, G. Fregonara, S. Trasatti, *Electrochimica Acta* **1990**, 35, 263; c) C. C. McCrory, S. Jung, J. C. Peters, T. F. Jaramillo, *J. Am. Chem. Soc.* **2013**, 135, 16977.

[5] a) N. T. Suen, S. F. Hung, Q. Quan, N. Zhang, Y. J. Xu, H. M. Chen, *Chem Soc Rev.* **2017**, 46, 337; b) X.-F. Lu, P.-Q. Liao, J.-W. Wang, J.-X. Wu, X.-W. Chen, C.-T. He, J.-P. Zhang, G.-R. Li, X.-M. Chen, *J. Am. Chem. Soc.* **2016**, 138, 8336.

[6] a) J. Suntivich, K. J. May, H. A. Gasteiger, J. B. Goodenough, Y. Shao-Horn, *Science* **2011**, 334, 1383; b) F. Cheng, J. Shen, B. Peng, Y. Pan, Z. Tao, J. Chen, *Nat Chem.* **2011**, 3, 79; c) K. L. Nardi, N. Yang, C. F. Dickens, A. L. Strickler, S. F. Bent, *Adv. Energy Mater.* **2015**, 5, 1500412; d) M. S. Burke, L. J. Enman, A. S. Batchellor, S. Zou, S. W. Boettcher, *Chem. Mater.* **2015**, 27, 7549; e) Y. Zhu, W. Zhou, J. Sunarso, Y. Zhong, Z. Shao, *Adv. Funct. Mater.* **2016**, 26, 5862; f) L. Xu, Q. Jiang, Z. Xiao, X. Li, J. Huo, S. Wang, L. Dai, *Angew. Chem. Int. Ed.* **2016**, 55, 5277.

[7] a) R. Subbaraman, D. Tripkovic, K. C. Chang, D. Strmcnik, A. P. Paulikas, P. Hirunsit, M. Chan, J. Greeley, V. Stamenkovic, N. M. Markovic, *Nat Mater.* **2012**, 11, 550; b) M. Gong, Y. Li, H. Wang, Y. Liang, J. Z. Wu, J. Zhou, J. Wang, T. Regier, F. Wei, H. Dai, *J. Am. Chem. Soc.* **2013**, 135, 8452; c) F. Song, X. Hu, *Nat. Commun.* **2014**, 5, 4477; d) L. Chen, X. Dong, Y. Wang, Y. Xia, *Nat. Commun.* **2016**, 7, 11741; e) J. Ping, Y. Wang, Q. Lu, B. Chen, J. Chen, Y. Huang, Q. Ma, C. Tan, J. Yang, X. Cao, Z. Wang, J. Wu, Y. Ying, H. Zhang, *Adv. Mater.* **2016**, 28, 7640; f) H. Jin, S. Mao, G. Zhan, F. Xu, X. Bao, Y. Wang, *J. Mater. Chem. A* **2017**, 5, 1078; g) J.-X. Feng, H. Xu, Y.-T. Dong, S.-H. Ye, Y.-X. Tong, G.-R. Li, *Angew. Chem. Int. Ed.* **2016**, 55, 3694; h) J.-X. Feng, S.-H. Ye, H. Xu, Y.-X. Tong, G.-R. Li, *Adv. Mater.* **2016**, 28, 4698.

[8] a) H. B. Yang, J. Miao, S. F. Hung, J. Chen, H. B. Tao, X. Wang, L. Zhang, R. Chen, J. Gao, H. M. Chen, L. Dai, B. Liu, *Sci. Adv.* **2016**, 2, e1501122; b) Z. Wang, Y. Lu, Y. Yan, T. Y. P. Larissa, X. Zhang, D. Wuu, H. Zhang, Y. Yang, X. Wang, *Nano Energy* **2016**, 30, 368; c) C. Hu, L. Dai, *Adv. Mater.* **2017**, 29.

[9] X. Long, J. Li, S. Xiao, K. Yan, Z. Wang, H. Chen, S. Yang, *Angew. Chem. Int. Ed.* **2014**, 126, 7714.

[10] a) A. Bhaumik, P. Mukherjee, R. Kumar, *J. Catal.* **1998**, 178, 101; b) Z. Lu, W. Zhu, X. Yu, H. Zhang, Y. Li, X. Sun, X. Wang, H. Wang, J. Wang, J. Luo, X. Lei, L. Jiang, *Adv. Mater.* **2014**, 26, 2683; c) C. Ling, Y. Huang, H. Liu, S. Wang, Z. Fang, L. Ning, *J. Phys. Chem. C* **2014**, 118, 28291; d) Y. Li, C. Zhao, *ACS Catal.* **2017**, DOI:

10.1021/acscatal.6b034972535.
[11] K. S. Lakhi, D. H. Park, K. Al-Bahily, W. Cha, B. Viswanathan, J. H. Choy, A. Vinu, *Chem Soc Rev* **2017**, 46, 72.
[12] a) T. Y. Ma, S. Dai, M. Jaroniec, S. Z. Qiao, *Angew. Chem. Int. Ed.* **2014**, 53, 7281; b) J. Duan, S. Chen, M. Jaroniec, S. Z. Qiao, *ACS Nano* **2015**, 9, 931.
[13] T. Y. Ma, Y. Tang, S. Dai, S. Z. Qiao, *Small* **2014**, 10, 2382.
[14] Y. Wang, X. Wang, M. Antonietti, *Angew. Chem. Int. Ed.* **2012**, 51, 68.
[15] a) Y. Zhang, A. Thomas, M. Antonietti, X. Wang, *J. Am. Chem. Soc.* **2009**, 131, 50; b) J. H. Lee, M. J. Park, S. J. Yoo, J. H. Jang, H. J. Kim, S. W. Nam, C. W. Yoon, J. Y. Kim, *Nanoscale* **2015**, 7, 10334; c) X. Du, G. Zou, Z. Wang, X. Wang, *Nanoscale* **2015**, 7, 8701.
[16] J. Yan, Z. Fan, W. Sun, G. Ning, T. Wei, Q. Zhang, R. Zhang, L. Zhi, F. Wei, *Adv. Funct. Mater.* **2012**, 22, 2632.
[17] L. Xu, Y.-S. Ding, C.-H. Chen, L. Zhao, C. Rimkus, R. Joesten, S. L. Suib, *Chem. Mater.* **2008**, 20, 308.
[18] B. Mavis, M. Akinc, *Chem. Mater.* **2006**, 18, 5317.
[19] S. Yang, Y. Gong, J. Zhang, L. Zhan, L. Ma, Z. Fang, R. Vajtai, X. Wang, P. M. Ajayan, *Adv. Mater.* **2013**, 25, 2452.
[20] L. Li, J. Qin, H. Bi, S. Gai, F. He, P. Gao, Y. Dai, X. Zhang, D. Yang, P. Yang, *Sci. Rep.* **2017**, 7, 43413.
[21] L. Ma, H. Fan, K. Fu, S. Lei, Q. Hu, H. Huang, G. He, *ACS Sustainable Chem. Eng.* **2017**, DOI: 10.1021/acssuschemeng.7b01312.
[22] M. Jing, C. Wang, H. Hou, Z. Wu, Y. Zhu, Y. Yang, X. Jia, Y. Zhang, X. Ji, *J. Power Sources* **2015**, 298, 241.
[23] W. Liu, C. Lu, X. Wang, K. Liang, B. K. Tay, *J. Mater. Chem. A* **2015**, 3, 624.
[24] B. Dong, M. Li, S. Chen, D. Ding, W. Wei, G. Gao, S. Ding, ACS Appl. Mater. Interfaces **2017**, DOI: 10.1021/acsami.7b02693.

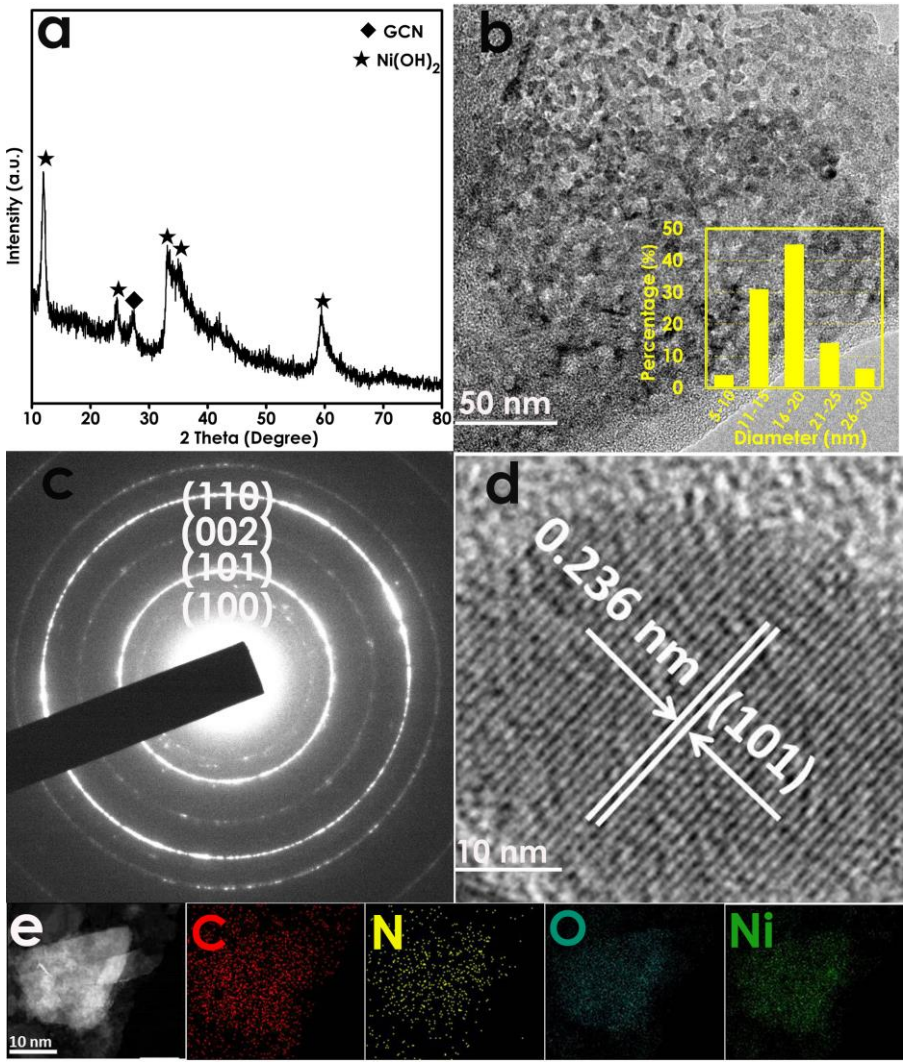

Figure 1. (a) XRD, (b) TEM image (inset: statistical result of the diameters of $Ni(OH)_2$ nanoplates), (c) SAED, (d) HRTEM, and (e) Dark-field STEM image and corresponding elemental mappings of GCNN:65.

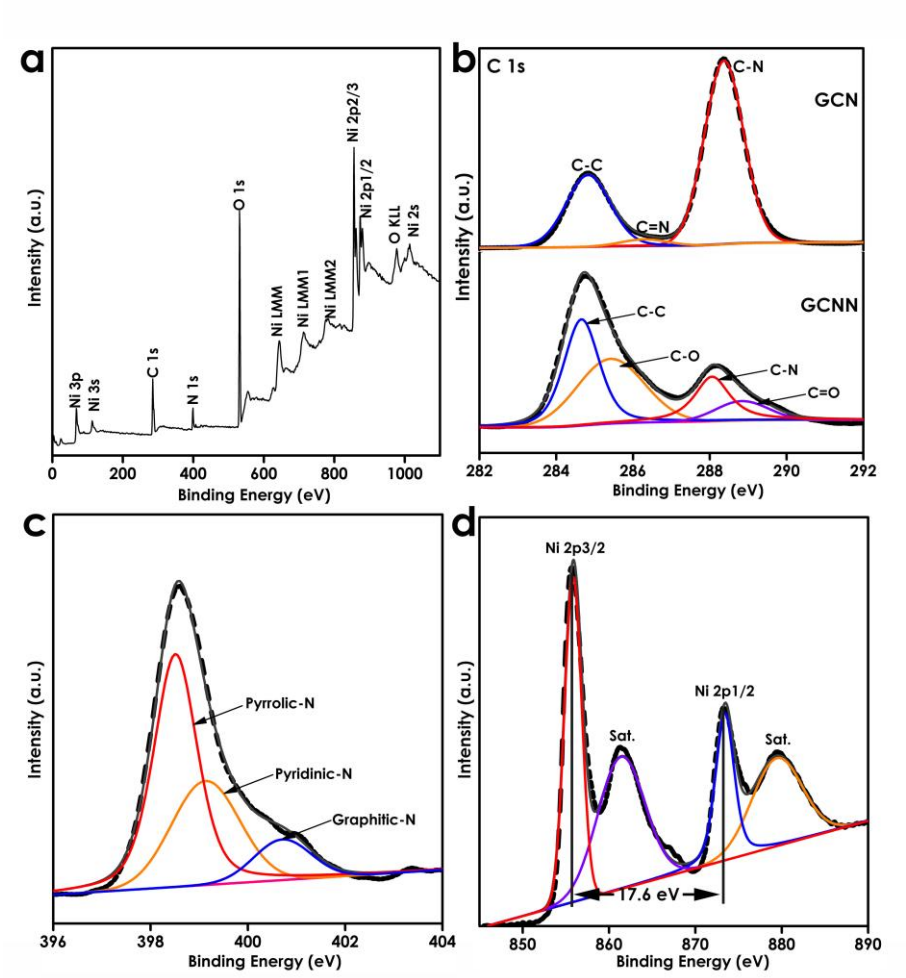

Figure 2. XPS spectra of GCNN:65: (a) survey spectrum, (b) C 1s, (c) N 1s and (d) Ni 2p.

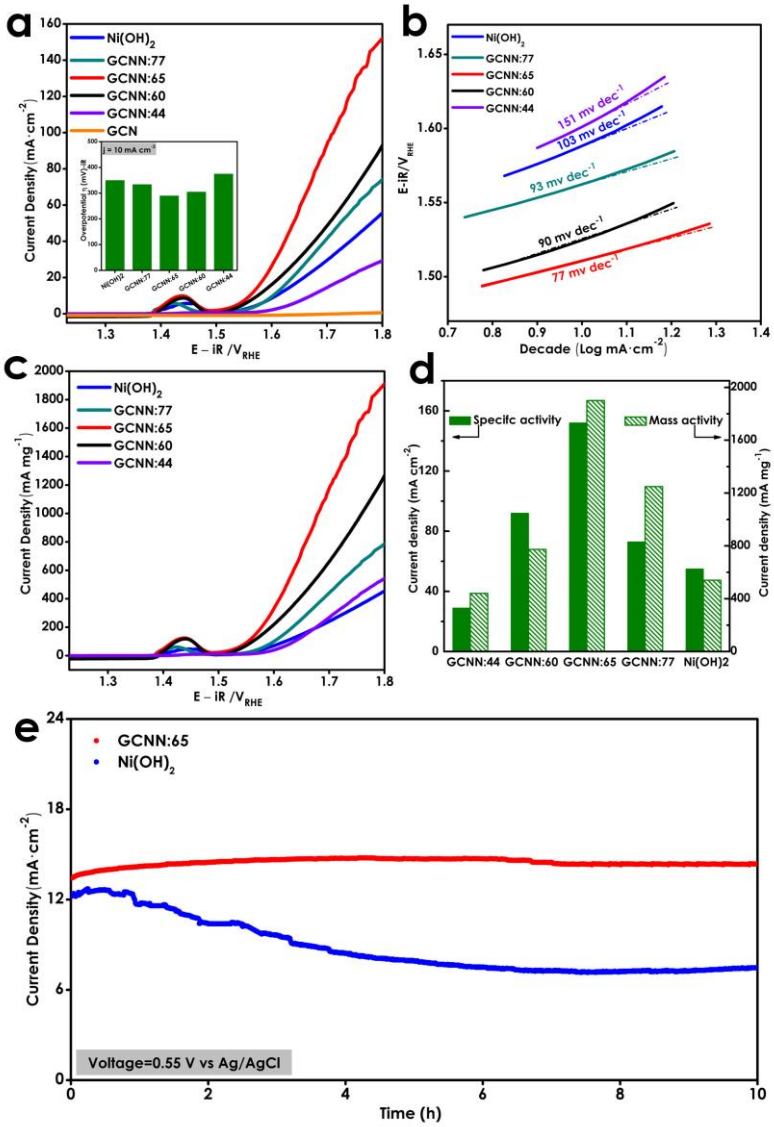

Figure 3. (a) LSV polarization curves measured at a scan rate of 5 mV s^{-1}. (b) Tafel plots (potential versus log(current density)) derived from LSV curves. (c) LSV curves plotted based on $Ni(OH)_2$ mass-normalized current density. (d) Current densities at 1.8 V vs. RHE. (e) Chronoamperometry at a constant potential of 0.55 V (vs. Ag/AgCl) without iR compensation.

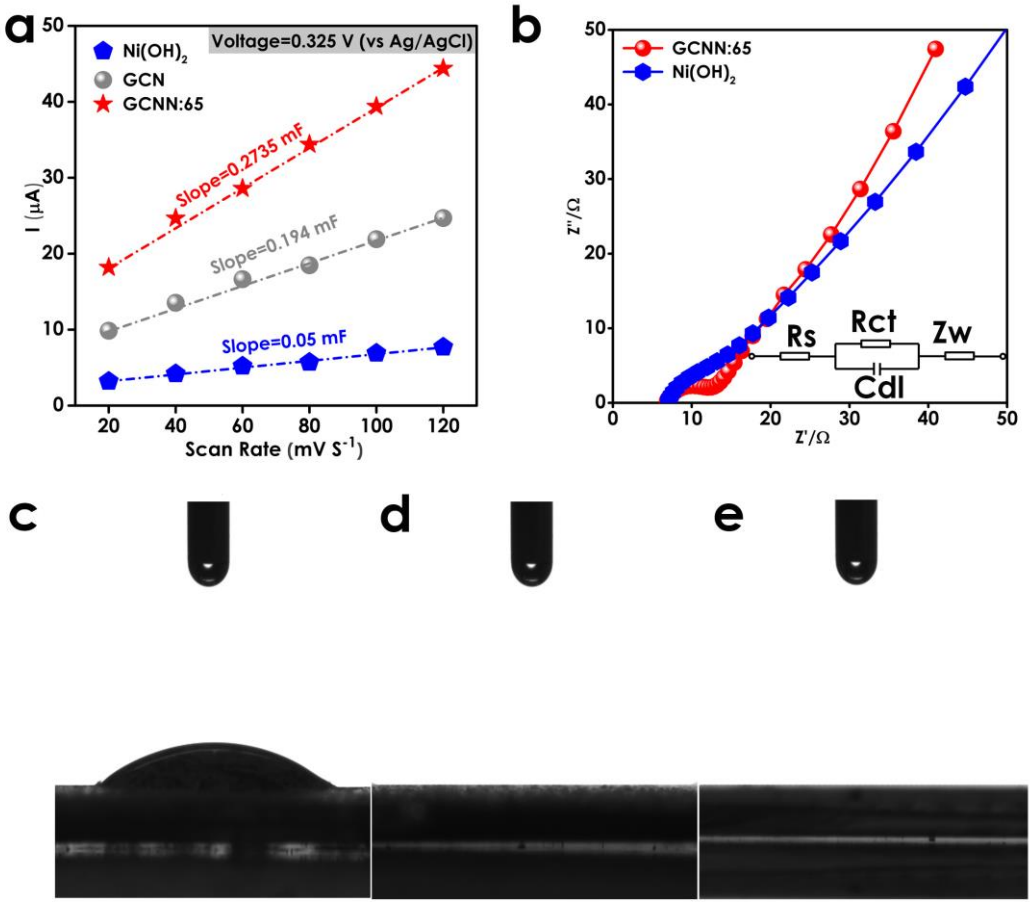

Figure 4. (a) The current at 0.325 V (vs. Ag/AgCl) versus scan rate measured in a non-Faradaic range. (b) Electrochemical impedance spectra of GCNN:65 and $Ni(OH)_2$ recorded at 0.6 V (vs. Ag/AgCl) (inset: equivalent circuit model). Contact angle measurements of $Ni(OH)_2$ (c), GCNN:65 (d), and GCNN (e).

Wettability matters: Electrochemically inert functionalized g-C_3N_4 can significantly enhance water oxidation catalysis by constructing a superhydrophilic catalyst surface and promoting substantial exposure of active sites. This work opens a new avenue for the development of highly efficient catalysts for electrochemical reactions taking place in aqueous and non-aqueous medium.

Keyword: Graphitic carbon nitride; Wettability; Nickel hydroxide; Oxygen evolution reaction

Yaping Chen, Qian Zhou, Guoqiang Zhao, Zhenwei Yu, Xiaolin Wang, Shi Xue Dou, Wenping Sun*

Title: Electrochemically Inert g-C_3N_4 Promotes Water Oxidation Catalysis

ToC figure